

Relativistic calculation of non-dipole effects in high harmonic generation

I. A. Ivanov^{1*} and Kyung Taec Kim^{1,2†}

¹ *Center for Relativistic Laser Science, Institute for Basic Science (IBS),*

Gwangju 61005, Republic of Korea and

²*Department of Physics and Photon Science, GIST, Gwangju 61005, Korea*

(Dated: October 20, 2023)

We present results of relativistic calculations of even order harmonic generation from various atomic targets. The even order harmonics appear due to the relativistic non-dipole effects. We take these relativistic effects into account by using an approach based on the solution of the time-dependent Dirac equation. The spectra of the non-dipole even harmonics look qualitatively similar to the spectra of the dipole harmonics obeying the same classical cutoff rule. The temporal dynamics of the formation of the non-dipole harmonics is, however, distinctly different from the process of dipole harmonics formation. Even order harmonics emission is strongly suppressed at the beginning of the laser pulse, and the emission times of the non-dipole harmonics are shifted with respect to the bursts of the dipole emission. These features are partly explained by a simple modification of the classical three-step model which takes into account selection rules governing the emission of harmonic photons.

I. INTRODUCTION

One can expect relativistic effects to play important role in the dynamics of the processes of atomic or molecular interactions with strong laser pulses for laser intensities over 10^{18} W/cm² [1], when, with increasing ponderomotive energy, electron velocity can approach speed of light in the vacuum. It has been realized since the pioneering paper by Reiss [2],

*Electronic address: igorivanov@ibs.re.kr

†Electronic address: kyungtaec@gist.ac.kr

however, that relativistic effects may reveal themselves even for moderately intense (10^{13} - 10^{14} W/cm²) low frequency infrared (IR) laser fields. For instance, even for the IR laser fields of intensity of the order of 10^{13} W/cm², the relativistic effects are visible in the photo-electron spectra [3–9] in the tunneling regime of ionization, characterized by the values $\gamma \lesssim 1$, where $\gamma = \omega \sqrt{2|I_p|}/E_0$ is the Keldysh parameter [10], and ω , E_0 and I_p are the field frequency, field strength and ionization potential of the target system expressed in atomic units. These relativistic non-dipole effects are due to the influence of the magnetic field component of the laser pulse which induces a non-negligible momentum transfer to the photoelectrons [11, 12]. Alternatively, if we prefer the photon picture of light, one might say that an IR photon carries small momentum, but a large number of the photons participating in the process of the tunneling ionization [13] deliver non-negligible momentum to the ionized electron [14, 15].

The momentum delivered by the photons to the photo-electron was measured experimentally under the typical parameters of the tunneling ionization regime [16]. This momentum manifests itself, on average, as a shift of the photo-electron momentum distributions (PMD) in the pulse propagation direction. More detailed picture, which emerges as a result of the complex interplay of the magnetic and Coulomb forces, includes the so-called direct electrons which never recollide with the parent ion and are driven in the direction of the laser photon momentum, and the slow electrons which experience recollisions and may acquire momentum opposite to the photon momentum [5].

Theoretical study of these effects clearly necessitates methods which go beyond the commonly used non-relativistic dipole approximation. A number of theoretical procedures allowing to consider the relativistic non-dipole effects have been described in the literature, including the relativistic strong-field approximation [8, 9, 17, 18], time-dependent Schrödinger equation (TDSE) with non-dipole corrections [6, 14, 15, 19], an approach based on the non-dipole strong-field-approximation Hamiltonian [20], and the time-dependent Dirac equation (TDDE) [21–24].

The non-dipole effects manifest themselves as well in other processes occurring when atoms or molecules interact with laser fields. The process which will interest us in the present work is the process of the High Harmonic Generation (HHG). The non-dipole effects are known to produce several modifications in the HHG spectra. It was found [25] that the non-dipole interactions lead to decrease of harmonic intensity and shift of odd order

harmonics in the spectra. A detailed investigation of the effect of the pulse magnetic field on harmonic spectra was reported in [26–28]. It was found [26] that the non-dipole magnetic field effects result in the emission of photons polarized along the propagation direction which, for the laser pulse wavelength of 800 nm and intensity of the order of 5×10^{15} W/cm², is several orders of magnitude weaker than the photon emission polarized parallel to the driving pulse polarization direction. For stronger pulses with the intensities of the order of 10^{17} W/cm², the magnetic field effects start playing crucial role [28]. Electron drift in the laser propagation direction due to the magnetic-field component of the laser pulse prevents recollisions, and hence, as one could expect on the basis of the picture provided by the celebrated three-step model of HHG [29, 30], leads to the decrease of the harmonic emission.

Perhaps one of the most striking manifestations of the non-dipole effects is appearance of even order harmonics in the HHG spectra [31–33], presenting an example of a relatively small perturbation producing not only relatively minor quantitative modifications of the spectra, but introducing a qualitative change: harmonics with frequencies forbidden in the dipole approximation. The appearance of the even order harmonics can be understood as a result of the break-up of the well-known symmetry which the electron trajectories responsible for the emission of the harmonic photons exhibit in the dipole approximation [29]. Magnetic field effects break this symmetry, and thus make possible generation of even order harmonics. These harmonics were studied theoretically in [32], using perturbative treatment of the non-dipole effects.

In the present paper we report a systematic theoretical study of the non-dipole effects, in particular generation of the even order harmonics, from various atomic targets. We use the TDDE as our main calculational tool, basing on the previously developed procedure for the numerical solution of the time-dependent Dirac equation [23, 24]. The approach based on the TDDE provides a complete non-perturbative description of the non-dipole, as well as other relativistic effects.

Atomic units with $\hbar = 1$, $e = 1$, $m = 1$, and $c \approx 137.036$ (here e and m are charge and mass of the electron, c - speed of light) are used throughout the paper.

II. THEORY

A. Numerical solution to the time-dependent Dirac equation

We solve the TDDE:

$$i \frac{\partial \Psi(r, t)}{\partial t} = \hat{H} \Psi(r, t) \quad (1)$$

following the procedure we described in [23, 24], which we briefly recapitulate below for the readers convenience. In Eq. (1) $\Psi(r, t)$ is a four-component bispinor and the Hamiltonian operator has a form:

$$\hat{H} = \hat{H}_{\text{atom}} + \hat{H}_{\text{int}} , \quad (2)$$

with:

$$\hat{H}_{\text{atom}} = c \boldsymbol{\alpha} \cdot \hat{\mathbf{p}} + c^2(\beta - I) + I V(r) , \quad (3)$$

and

$$\hat{H}_{\text{int}} = c \boldsymbol{\alpha} \cdot \hat{\mathbf{A}} , \quad (4)$$

In Eq. (3):

$\boldsymbol{\alpha} = \begin{pmatrix} \mathbf{0} & \boldsymbol{\sigma} \\ \boldsymbol{\sigma} & \mathbf{0} \end{pmatrix}$, $\beta = \begin{pmatrix} I & \mathbf{0} \\ \mathbf{0} & -I \end{pmatrix}$, $I = \begin{pmatrix} I & \mathbf{0} \\ \mathbf{0} & I \end{pmatrix}$, $\boldsymbol{\sigma}$ are Pauli matrices, $\mathbf{0}$ and I are 2×2 null and identity matrices, $V(r)$ is the atomic potential and $c = 137.036$ - the speed of light. We subtracted from the field-free atomic Hamiltonian (3) the constant term Ic^2 corresponding to the rest mass energy of the electron.

We use a laser pulse linearly polarized in z - and propagating in x - directions. The vector potential of the pulse is defined in terms of the pulse electric field:

$$\mathbf{A}(x, t) = -\hat{\mathbf{e}}_z \int_0^u E(\tau) d\tau , \quad (5)$$

where $u = t - x/c$. At any given point in space the pulse has a finite duration T_1 so that $E(\tau)$ in Eq. (5) is non-zero only for $0 < \tau < T_1$. As targets, we will consider below a model atom with a short range (SR) Yukawa-type potential $V(r) = -1.903e^{-r}/r$, hydrogen

atom, and helium atom described by means of an effective potential [34]. The target atom is initially in the ground s -state $|\phi_0\rangle$ with the ionization potential (IP) of 0.5 a.u. for the hydrogen and Yukawa atoms and IP of 0.902 a.u. for the He atom.

The solution to Eq. (1) is expanded as a series in the basis bispinors:

$$\Psi(\mathbf{r}, t) = \sum_{l=j\pm 1/2}^j \sum_{M=-j}^j \Psi_{j l M}(\mathbf{r}, t), \quad (6)$$

where:

$$\Psi_{j l M}(\mathbf{r}, t) = \begin{pmatrix} g_{j l M}(r, t) \Omega_{j l M}(\mathbf{n}) \\ f_{j l M}(r, t) \Omega_{j l' M}(\mathbf{n}) \end{pmatrix}, \quad (7)$$

and the two-component spherical spinors are defined as $\Omega_{j l M}(\mathbf{n}) = \begin{pmatrix} C_{l, M-\frac{1}{2}, \frac{1}{2}}^{j M} Y_{l, M-\frac{1}{2}}(\mathbf{n}) \\ C_{l, M+\frac{1}{2}, \frac{1}{2}}^{j M} Y_{l, M+\frac{1}{2}}(\mathbf{n}) \end{pmatrix}$, (here $C_{l m \frac{1}{2} \mu}^{j M}$ are the Clebsch-Gordan coefficients, $Y_{l m}(\mathbf{n})$ -spherical harmonics, and $\mathbf{n} = \mathbf{r}/r$). Parameters l and l' in Eq. (6) must satisfy the relation $l + l' = 2j$.

To take into account the non-dipole effects due to the spatial dependence of the laser fields, vector potential (5) is expanded in a series of spherical harmonics at every time-step of the integration procedure. Substituting expansion (6) and expansion for the vector potential in the TDDE (1), and using well-known properties of spherical spinors [35, 36], one obtains a system of coupled differential equations for the radial functions $g_{j l M}(r, t)$ and $f_{j l M}(r, t)$ in Eq. (7). This system has been solved using a relativistic generalization of the well-known matrix iteration method (MIM) [37], which we described in detail in [23].

Appropriate choice of the propagation technique is essential, as the Dirac equation, as it is well-known, possesses some properties which are absent in the case of the non-relativistic wave-equation. These properties are due to the presence of the continuum of the negative energy states in the Dirac Hamiltonian which makes the Dirac Hamiltonian unbounded from below. One problem which this fact entails is the well-known problem of the collapse to the negative energies continuum [38], which may manifest itself when basis set methods are used to construct approximations to the bound states of the Dirac Hamiltonian [38]. We avoid this problem, since we do not rely on the basis set methods. Initial state of the system is prepared in our calculation by solving numerically the eigenvalue equation for the

field-free Dirac Hamiltonian employing shooting method. A related problem is the so-called Zitterbewegung problem [39]. Presence of a superposition of the states with positive and negative energies implies that a solution to the TDDE should exhibit very fast oscillations with characteristic frequencies of the order of c^2 . Such oscillations are indeed present and we can reproduce them in the framework of our numerical procedure by using sufficiently small integration time-step Δ [23]. We had to use the time-step Δ of the order of 10^{-6} a.u. in [23] to reproduce these oscillations. Use of such small values for Δ , if it were imperative, would make any practical calculations impossible, of course. Fortunately, one can bypass this problem by using an appropriate time-propagation technique. We discussed this issue in greater detail in [23, 40]. For readers convenience we present a core of the argument below. From the purely numerical point of view, presence of the fast oscillating terms in a system of the ordinary differential equations (ODE) gives us an example of a numerically stiff system of ODE, i.e. a system in which vastly different time-scales are present. To solve such a system of ODE we must use a stable integration method [41], which ensures that while the numerical solution does not reproduce very fast oscillations, it describes accurately the overall behavior of the true solution. The integration procedure that we use provides such a stability. We can illustrate this point using a simple example of a stiff system of two ODE:

$$i\dot{\mathbf{y}} = \mathbf{A} \cdot \mathbf{y}, \quad (8)$$

with Hermitian matrix $\mathbf{A} = \text{diag}(\lambda_1(t), \lambda_2(t))$. To mimic the problem at hand let us assume that λ_1 is of order of 1, while λ_2 has large negative value on the interval of time that we consider. Short-time propagator in the MIM method is a unitary Crank-Nicholson (CN) propagator [42], which relates solution vectors $\mathbf{y}_{n+1} = \mathbf{y}(t_{n+1})$ and $\mathbf{y}_n = \mathbf{y}(t_n)$ at times t_n and $t_{n+1} = t_n + \Delta$ as follows:

$$\mathbf{y}_{n+1} = \frac{1 - \frac{i\Delta}{2}\mathbf{A}(t_{n+1/2})}{1 + \frac{i\Delta}{2}\mathbf{A}(t_{n+1/2})}\mathbf{y}_n, \quad (9)$$

where $t_{n+1/2} = t_n + \Delta/2$. One can see from Eq. (9) that if at the n -th step of the propagation the second component of the vector \mathbf{y} acquires a numerical error $\delta y_n^{(2)}$, the unitarity of the CN propagation matrix in Eq. (9) makes this error remain bounded for $m > n$.

Spatial variables in the coupled differential equations for the radial functions $g_{jLM}(r, t)$ and $f_{jLM}(r, t)$ were discretized on a grid with the step size $\delta r = 0.05$ a.u., the radial variable was restricted to an interval $(0, R_{\max})$, with $R_{\max} = 400$ a.u., and angular momenta j up to 70 were included in the expansion (6) in the calculations below. The propagation time-step Δ was 0.05 a.u. Before proceeding to the description of the results of this calculation, it is instructive, however, to discuss an alternative treatment of the non-dipole effects based on the leading order perturbation theory (LOPT) expansion, as it provides a more transparent physical picture of the non-dipole effects than the complete Dirac equation. LOPT calculation described below was also used as an accuracy test for our solution to the TDDE.

B. LOPT treatment of the non-dipole effects.

We are interested in a LOPT solution to the TDDE considering the non-dipole effects as relativistic corrections.

The leading order relativistic corrections describing the non-dipole effects in atom-field interaction can be obtained by expanding the minimal coupling atom-field interaction Hamiltonian [5, 43, 44] in the velocity gauge:

$$\hat{H}_{\text{int}}^{\text{min}}(t) = \hat{\mathbf{p}} \cdot \mathbf{A}(\mathbf{r}, t) + \frac{\hat{\mathbf{A}}^2(\mathbf{r}, t)}{2} \quad (10)$$

in powers of c^{-1} [6]:

$$\hat{H}_{\text{min}}(t) = \hat{p}_z A(t) + \frac{\hat{v}_z x E(t)}{c} + \frac{A^2(t)}{2} + O(c^{-2}), \quad (11)$$

where $E(t) = -\frac{\partial A(t)}{\partial t}$ is the electric field of the pulse, and the velocity operator $\hat{\mathbf{v}} = \hat{\mathbf{p}} + \mathbf{A}(t)$ has been introduced. The last term on the r.h.s. of Eq. (11) is a function of time only and can be removed by a unitary transformation of the wave-function.

Including spin effects in the interaction Hamiltonian is not necessary, if we are interested in the effects of the leading order in powers of c^{-1} [5, 25]. The fact that the spin degrees of freedom can be neglected in the leading order of the c^{-1} expansion, can be understood using the semi-classical picture of the spin effects, in which additional force due to the presence of the spin degrees of freedom, acting on the electron, is $\mathbf{F} = -\nabla U_m$, where $U_m = -\boldsymbol{\mu} \cdot \mathbf{H}$, energy of the spin-magnetic field interaction. Here \mathbf{H} is the magnetic field and $\boldsymbol{\mu}$ is electron's

magnetic moment related to the expectation value of electron's spin $\boldsymbol{\mu} = -2\mathbf{S}/c$. Spatial gradient of \mathbf{H} introduces an additional factor of c^{-1} , making contribution of the force \mathbf{F} an effect of higher order in c^{-1} . As for the relativistic corrections to the field-free atomic Hamiltonian, the so-called Breit-Pauli Hamiltonian [44], it adds terms of the order of c^{-2} to the non-relativistic atomic Hamiltonian. We do not have, therefore, to include these corrections in the LOPT treatment. To the leading order in powers of the c^{-1} -expansion, the dynamics of the system can thus be described by the time-dependent Schrödinger equation (TDSE):

$$i\frac{\partial\Psi(\mathbf{r},t)}{\partial t} = \left(\hat{H}_{\text{atom}} + \hat{H}_{\text{d}}(t) + \hat{H}_{\text{nd}}(t)\right)\Psi(\mathbf{r},t), \quad (12)$$

where

$$\hat{H}_{\text{atom}} = \frac{\hat{\mathbf{p}}^2}{2} + V(r) \quad (13)$$

is atomic field-free Hamiltonian,

$$\hat{H}_{\text{d}}(t) = \hat{p}_z A(t) \quad (14)$$

is the dipole part of the atom-field interaction and

$$\hat{H}_{\text{nd}}(t) = \frac{\hat{v}_z x E(t)}{c} \quad (15)$$

is the non-dipole part of the atom-field interaction containing the effects of the order of c^{-1} .

It is easy to check that the LOPT solution to the equation (12), with the non-dipole term (15) considered as a perturbation, can be written as:

$$\Psi^{\text{LOPT}}(\mathbf{r},t) = \Psi_{\text{d}}(\mathbf{r},t) + \Psi_{\text{nd}}^{(1)}(\mathbf{r},t), \quad (16)$$

where the LOPT non-dipole correction is given by the expression:

$$\Psi_{\text{nd}}^{(1)}(\mathbf{r},t) = -i \int_0^t \hat{U}_{\text{d}}(t,\tau) \hat{H}_{\text{nd}}(\tau) \Psi_{\text{d}}(\mathbf{r},\tau) d\tau. \quad (17)$$

As can be seen from Eq. (15) for the operator \hat{H}_{nd} this correction is of the order of c^{-1} . In Eq. (16) and Eq. (17) $\Psi_{\text{d}}(\mathbf{r},t)$ is the zero-order solution to the non-relativistic

TDSE taking into account only the dipole part of the atom-field interaction, $\hat{U}_d(t, \tau)$ is the evolution operator describing evolution of the system driven by the non-relativistic dipole Hamiltonian. $\hat{U}_d(t, \tau)$ satisfies the operator equation:

$$i \frac{\partial \hat{U}_d(t, \tau)}{\partial t} = \left(\hat{H}_{\text{atom}} + \hat{H}_d(t) \right) \hat{U}_d(t, \tau) , \quad (18)$$

and the initial condition $\hat{U}_d(\tau, \tau) = \hat{I}$. In practice, we need not solve the operator equation (18). All we have to do to compute the expression under the integral on the r.h.s of Eq. (16) for given τ and t , is to propagate first the initial state wave-function on the interval $(0, \tau)$ using the non-relativistic TDSE with the Hamiltonian (14), obtaining thus a state vector $\Psi_d(\tau)$. We act than on this vector with the operator $\hat{H}_{\text{nd}}(\tau)$ and propagate it further in time till the moment t . The non-relativistic TDSE was solved using the well-tested numerical procedure described in [45].

C. Calculation of electron velocity and HHG spectra

Once the solution to the TDDE (1) is obtained, expectations value of the electron velocity can be obtained as [46]:

$$\mathbf{v}(t) = c \langle \Psi(t) | \boldsymbol{\alpha} | \Psi(t) \rangle . \quad (19)$$

Harmonic spectra can then be calculated using the usual semi-classical approach, in which the spectral intensity of the harmonic emission can be expressed in terms of the Fourier transform of electron's velocity:

$$S_a(\Omega) \propto \left| \int_0^{T_1} v_a(t) W(t) e^{i\Omega t} dt \right|^2 . \quad (20)$$

where $v_a(t)$ is either x - or z - component of the electron velocity for the non-dipole and dipole harmonic intensities $S_x(\Omega)$ and $S_z(\Omega)$, respectively. In the velocity form for the harmonics intensity which we use here, we do not need to introduce additional powers of harmonic frequency, which would be present had we used length or acceleration forms [47]. The factor $W(t)$ in Eq. (20) is the window function [48], for which we employ the Hann form: $W(t) = \sin^2 \left(\frac{\pi t}{T_1} \right)$.

The most noticeable effects which the relativistic non-dipole corrections produce are appearance of harmonic photons polarized in the laser propagation direction [26–28] and appearance of even order harmonics in the HHG spectra [33, 49]. The LOPT picture allows to explain these features transparently. Substituting the expression Eq. (16) for the LOPT wave-function into the matrix element:

$$\langle \Psi^{\text{LOPT}}(t) | \hat{\mathbf{v}} | \Psi^{\text{LOPT}}(t) \rangle \approx \hat{\mathbf{x}}v_x(t) + \hat{\mathbf{y}}v_y(t) + \hat{\mathbf{z}}v_z(t) , \quad (21)$$

defining the leading order contributions to the expectation value of electron velocity, one obtains:

$$v_z(t) = \langle \Psi_d(t) | \hat{v}_z | \Psi_d(t) \rangle . \quad (22)$$

For the geometry we use, the evolution operator $\hat{U}_d(t, \tau)$ commutes with \hat{l}_z - the z - component of the angular momentum, i.e., it is a conserved quantity for the quantum evolution driven by the dipole Hamiltonian (13) and (14). \hat{l}_z , therefore, has a definite value $l_z = 0$ in the state described by the wave-function $\Psi_d(t)$, and the matrix element $\langle \Psi_d(t) | \hat{v}_x | \Psi_d(t) \rangle$ vanishes because of the well-known dipole selection rules [44]. Leading order contribution to $v_x(t)$, is, therefore, of the order of c^{-1} , and is given by the expression:

$$\begin{aligned} v_x(t) &= \langle \Psi_d(t) | \hat{v}_x | \Psi_{\text{nd}}^{(1)} \rangle + \langle \Psi_{\text{nd}}^{(1)}(t) | \hat{v}_x | \Psi_d \rangle \\ &= 2\text{Re} \langle \Psi_d(t) | \hat{v}_x | \Psi_{\text{nd}}^{(1)} \rangle \\ &= 2\text{Im} \left(\int_0^t \langle \Psi_d(t) | \hat{p}_x \hat{U}_d(t, \tau) \hat{H}_{\text{nd}}(\tau) | \Psi_d(\tau) \rangle d\tau \right) . \end{aligned} \quad (23)$$

In the last line of Eq. (23) we used expression (17) for $\Psi_{\text{nd}}^{(1)}$. The same dipole selection rules [44] and the structure of Eq. (17) ensure that the contribution of the order of c^{-1} to $v_y(t)$ is zero. The leading contribution of the non-dipole effects is, therefore, non-zero only for the x -component of the electron velocity. Orientation of the dipole velocity due to this relativistic contribution results, thus, in the appearance of the harmonic photons polarized in the propagation direction in accordance with the observations made in [26–28].

As we mentioned above, the appearance of the even order harmonics can be understood as a result of violation of the symmetry of the electron trajectories responsible for the emission

of harmonic photons in the dipole approximation [29]. From the LOPT perspective this effect can be explained as follows. As one can see from Eq. (14) and Eq. (15), the dipole interaction operator (14) has odd parity, i.e. it couples states of different parities, while the non-dipole operator (15) has even parity. Employing a somewhat lousy language, we might say that the presence of these two atom-field interaction Hamiltonians can be described as the presence of two kinds of photons: the "dipole" photons and the "non-dipole" photons, whose emission and absorption are governed by the operators (14) and (15), respectively. Using these notions and the LOPT expression for $v_x(t)$ in Eq. (23), contribution of the non-dipole interaction to the formation of the N -th harmonic can be described as absorption of $N - 1$ "dipole" photons and one "non-dipole" photon, with subsequent recombination to atomic ground state accompanied by emission of a harmonic photon with frequency $N\omega$. Using the informal terminology which we adopted, one might say that the emitted harmonic photon is of the "dipole" nature since spontaneous emission satisfies the dipole selection rules. Conservation of the total parity for the combined system of atom and the "dipole" and the "non-dipole" photons implies then that N must necessarily be even.

Besides providing a simple physical picture of the appearance of even harmonics, the LOPT approach which we described above, can be used as a test of the accuracy of our solution to the TDDE. To do such a test we performed calculations of the expectation values of electron velocity using TDDE and LOPT approaches for the cosine-pulse form shown in Fig. 1, with the vector potential in Eq. (5) given by the equation: $\mathbf{A}(x, t) = -\mathbf{e}_z \frac{E_0}{\omega} \sin^2\left(\frac{\pi u}{T_1}\right) \sin \omega u$ where $\omega = 0.057$ a.u., $E_0 = 0.0534$ a.u., $u = t - x/c$. A comparison of the TDDE results obtained using Eq. (19) and the LOPT results obtained using Eq. (23) for the x - component of electron velocity is shown in Fig. 2. The results of the LOPT treatment prove to be virtually identical to the results of the TDDE calculation which is not surprising given that the relativistic corrections could be expected to be small for the field parameters we consider.

III. RESULTS

We report below results which we obtained from our TDDE calculations for dipole $S_z(\Omega)$ and non-dipole $S_x(\Omega)$ harmonic intensities for different targets. HHG spectra were obtained by computing electron velocity as prescribed by Eq. (19) and using Eq. (20) to compute

harmonic intensities. Calculations were performed using the sine waveform shown in Fig. 1 with the electric field given by the equation: $E(u) = E_0 \sin^2\left(\frac{\pi u}{T_1}\right) \sin \omega u$. We report below results for the base frequencies $\omega = 0.114$ a.u. (wavelength of 400 nm) and $\omega = 0.057$ a.u. (wavelength of 800 nm).

In Fig. 3 we show HHG spectra that we obtained for the driving pulse wavelength $\lambda = 400$ nm and different field strengths for various targets. Fig. 3 shows both dipole $S_z(\Omega)$ and non-dipole $S_x(\Omega)$ harmonic intensities. The vertical lines in the Figures show positions of the classical cutoffs given by the well-known $3.17U_p + I_p$ (here $U_p = E_0^2/4\omega^2$ and I_p are ponderomotive and ionization energies respectively) rule of the three-step model [29, 30]. In Fig. 4 we zoom on the parts of the harmonic spectra more closely to demonstrate the presence of odd and even harmonics in the dipole and non-dipole spectra respectively.

Quite expectedly, behavior of the dipole intensity $S_z(\Omega)$ shown in Fig. 3 agrees very well with the three-step model predictions, exhibiting a sharp drop in magnitude after reaching the classical cutoff. The non-dipole $S_x(\Omega)$ spectra mimic this behavior very closely. This may be not surprising if we make use again of the LOPT picture of formation of the non-dipole harmonics we presented above, which relied on the notions of 'dipole' and 'non-dipole' photons with operators describing their interactions with an atom given by Eq. (14) and Eq. (15), respectively. We remind, that in the framework of this picture the N -th non-dipole harmonic is produced as a result of the absorption of $N - 1$ "dipole" photons and one "non-dipole" photon. As far as the harmonic spectra are concerned, the mechanism responsible for the formation of the non-dipole harmonic emission differs thus from the mechanism of the emission of the dipole harmonics only in the replacement of one 'dipole' photon with a 'non-dipole' one. This replacement leads to the replacement of the odd order harmonics in the spectra by the even order ones and results in an overall drop in magnitude in the harmonic spectra due to the presence of the additional factor of c^{-1} in the non-dipole interaction operator (15).

The energy and parity conservation considerations which lead us to the general conclusions about the character of the non-dipole spectra do not tell us anything about temporal dynamics of the formation of the non-dipole harmonics. We can have a glimpse of this temporal dynamics by analyzing Gabor transforms [50] of dipole and non-dipole velocities:

$$T_a(\Omega, t) = \int_0^{T_1} v_a(\tau) \Phi^*(t, \tau, \Omega) d\tau, \quad (24)$$

where $\Phi(t, \tau, \Omega) = \exp \{i\Omega\tau - (t - \tau)^2/2(x_0T)^2\}$, parameter x_0 determines resolution in the temporal domain, and T is an optical cycle of the laser field. Gabor transform, as well as closely related wavelet transform, allows us to take a look simultaneously at both time and frequency domains, and allows to determine, in particular, when different harmonics are emitted [51–53]. We used $x_0 = 0.1$ in the calculations below. This value of x_0 gives us rather poor resolution in the frequency domain, but high resolution in the time domain, which is of interest to us presently.

The absolute values $|T_a(\Omega, t)|$ for both dipole and non-dipole velocities are shown in Fig. 5 and Fig. 6 for the SR Yukawa and hydrogen atoms. One can see that, dynamically, formation of dipole and non-dipole harmonics proceeds quite differently. For both Yukawa and hydrogen atoms systems emission of the non-dipole harmonics is strongly suppressed at the early stages of pulse development, and emission times for the non-dipole harmonics are shifted with respect to the dipole radiation bursts. Such behavior could be anticipated by looking at Fig. 2 which shows that x - component of the velocity starts actually respond to the field only for times approaching the midpoint of the pulse. The reason for this could be traced back to the character of the fully quantum expression for the velocity component v_x in the second LOPT equation (23), with time integration on the right-hand side of this equation smoothing out high frequency oscillations. To elucidate this issue further we performed a simple classical calculation of the emitted photon energy as a function of the recombination time using the physical picture provided by the three-step model. We assume that electron is ionized at the moment of time t_{ion} and returns to the parent ion at the moment of time t_{ret} , emitting a harmonic photon with energy $E_{ret} + I_p$. As is usually assumed in the three-step model calculations, we consider only the effect of the external field (5) on the electron motion, neglecting completely ionic potential. The only difference of our calculation and the traditional three-step model analysis of the harmonic emission, is that we take into account effect of the Lorentz force due to the magnetic field of the pulse. We simulate electron motion in a plane (which is the (x, z) - plane for the geometry we employ), solving the set of the classical Newton equations, which for the fields configuration, geometry and atomic units system we employ, can be written as:

$$\begin{aligned}
\ddot{x} &= -\frac{v_z}{c}E(t) \\
\ddot{z} &= -E(t) + \frac{v_x}{c}E(t)
\end{aligned}
\tag{25}$$

Following the prescription of the traditional three-step model we solve equations (25) with zero initial conditions imposed at the ionization time: $v_x(t_{ion}) = v_z(t_{ion}) = 0$ and $x(t_{ion}) = z(t_{ion}) = 0$. We assume that the electron trajectory returns to the origin, if at the moment of time t_{ret} , z -coordinate of the electron trajectory changes sign.

Fig. 7(a) shows results of such a simulation, which qualitatively agree with the dynamics of the dipole harmonics emission shown in Fig. 5 and Fig. 6, with bursts of harmonics emission occurring every half cycle of the laser pulse. To be able to apply this classical analysis to the emission of the non-dipole harmonics we must, however, introduce one essentially quantum ingredient in the model described by the classical equations(25). Emission of the non-dipole radiation differs from the emission of the dipole harmonics in one important aspect. For the geometry we employ, the dipole harmonics photon emission process satisfies selection rule $\Delta M = 0$, where M is the z - projection of the electron angular momentum. On the other hand, emission of the non-dipole harmonic photon, as can be seen from the LOPT analysis we presented above, must satisfy selection rule $\Delta M = \pm 1$. This means that for the ground s - state that we consider, non-dipole radiation can be emitted only by electrons with non-zero angular momentum. We can incorporate this fact in our classical model by introducing a filter parameter f in the simulations, and considering only those returning trajectories for which at the moment of time t_{ret} squared classical angular momentum value exceeds the threshold value set by the filter parameter f . Results of such calculations are shown in Fig. 7(b-d) for different values of the filter parameter f . One can see that by increasing the value of the filter parameter, we make the classical picture in Fig. 7 look more like the Gabor transform results shown in Fig. 5 and Fig. 6. In particular, Fig. 7(c-d) show the absence of the non-dipole harmonics emission during the first two cycles of the laser pulse, the feature which is also demonstrated by the quantum analysis based on the Gabor transform in Fig. 5 and Fig. 6. Applying non-zero filter parameter does not change, however, the maximum energy E_{ret} of the returning electron, which explains why non-dipole harmonic emission spectra exhibit essentially the same cutoffs as the dipole

harmonic emission spectra. This simple classical picture of the formation of the non-dipole harmonics, which takes as quantum ingredient only the requirement that the electron angular momentum on the returning trajectories should exceed certain threshold value, agrees, thus, qualitatively with the fully quantum picture.

We also performed TDDE calculations for the pulse base frequency $\omega = 0.057$ a.u. (corresponding to the wavelength of 800 nm). In Fig. 8 and Fig. 9 we show harmonic spectra we obtain from TDDE for the SR Yukawa and hydrogen atoms. Fig. 10 shows results of the analysis of the temporal dynamics of the harmonic formation based on the Gabor transform (24). These Figures show essentially the same picture as the results we presented above for the driving pulse wavelength of 400 nm. The spectra of the non-dipole harmonics follow closely the classical dipole cutoff rule, and differ in this respect from the dipole emission spectra only in their intensity. Temporal pictures of the harmonics formation in the dipole and the non-dipole cases are, however, totally different. The main difference is, just as in the case of the driving pulse wavelength of 400 nm, the absence of the harmonic emission at the early stages of the pulse development, the feature which we explained above using the results of the classical calculations shown in Fig. 7(c,d).

The factor which is responsible for the difference in intensity between the dipole and non-dipole harmonics is the additional factor of c^{-1} which, as one can see from Eq. (23) and Eq. (15), is present in the LOPT formula for the x -component of the velocity. The presence of this factor in v_x leads to a dampening factor of c^{-2} in the expression for the non-dipole harmonics intensity. It is rather difficult to obtain a more detailed insight about relative magnitude of the dipole and non-dipole harmonic intensities from the cumbersome LOPT expressions Eq. (22) and Eq. (23). One can, however, obtain a simple estimate using the reasoning based not on the Schrödinger picture that we have used so far, but on the equivalent Heisenberg picture of the quantum mechanics (QM). In the latter, we remind, the operators evolve in time, while the state vectors do not. We obtain, of course, the same expectation values for all physical observables in both pictures.

In the Heisenberg picture time-evolution of the operators $\hat{\mathbf{r}}(t)$ and $\hat{\mathbf{p}}(t)$ is described by the equations [54]: $i\dot{\hat{\mathbf{r}}} = [\hat{\mathbf{r}}, \hat{H}]$, $i\dot{\hat{\mathbf{p}}} = [\hat{\mathbf{p}}, \hat{H}]$, where the Hamiltonian operator in our problem is $\hat{H} = \hat{H}_{\text{atom}} + \hat{H}_{\text{d}}(t) + \hat{H}_{\text{nd}}(t)$, with \hat{H}_{atom} , $\hat{H}_{\text{d}}(t)$ and $\hat{H}_{\text{nd}}(t)$ given by Eq. (13), Eq. (14), and Eq. (15), respectively. Calculating the commutators, one obtains the following equations of motion:

$$\begin{aligned}
\dot{\hat{x}} &= \hat{p}_x \\
\dot{\hat{p}}_x &= -i[\hat{p}_x, \hat{V}] - \frac{\hat{v}_z}{c}E(t) \\
\dot{\hat{z}} &= \hat{p}_z + A(t) + \frac{\hat{x}}{c}E(t) \\
\dot{\hat{p}}_z &= -i[\hat{p}_z, \hat{V}] ,
\end{aligned} \tag{26}$$

where \hat{V} is atomic potential operator, $\hat{v}_z = \hat{p}_z + A(t)$, $A(t)$ and $E(t)$ are the vector potential and the electric field of the pulse. Eq. (26) is the quantum-mechanical analogue of the classical equations describing electron motion in the potential V in presence of the Lorenz force. It contains the same physical information and is, therefore, equivalent to the LOPT equations Eq. (22) and Eq. (23), but it provides a more clear physical picture and can be used as a starting point for making simplifying assumptions.

From the first two equations (26) one obtains:

$$\ddot{\hat{x}} = -i[\hat{p}_x, \hat{V}] - \frac{\hat{v}_z}{c}E(t) , \tag{27}$$

We will make an assumption that one can omit the commutator $[\hat{p}_x, \hat{V}]$ in Eq. (27). Some justification for this operation can be provided in the case of the SR Yukawa atom, when potential function $V(\mathbf{r})$ is effectively zero everywhere excepting a small neighborhood of the atom. We obtain then from Eq. (27) a relation for the expectation values of the electron acceleration $a_x = \langle \phi_0 | \ddot{\hat{x}} | \phi_0 \rangle$ and velocity $v_z = \langle \phi_0 | \hat{v}_z | \phi_0 \rangle$:

$$a_x = -\frac{v_z}{c}E(t) , \tag{28}$$

where $|\phi_0\rangle$ is the initial atomic state, which does not evolve in time in the Heisenberg picture. Assuming further that $E(t)$ is a monochromatic wave: $E(t) = E_0 \cos \omega t$ and calculating Fourier transforms of both sides of Eq. (28), we obtain a relation between the Fourier transforms $\tilde{v}_x(\Omega) = \int v_x(t) e^{i\Omega t} dt$ and $\tilde{v}_z(\Omega) = \int v_z(t) e^{i\Omega t} dt$:

$$-i\Omega \tilde{v}_x(\Omega) = \frac{E_0}{2c} (\tilde{v}_z(\Omega + \omega) + \tilde{v}_z(\Omega - \omega)) , \tag{29}$$

from which, using the fact that for any complex numbers z_1, z_2 : $|z_1 + z_2|^2 \leq (|z_1| + |z_2|)^2$, we obtain an inequality:

$$\Omega^2 S_x(\Omega) \leq \frac{E_0^2}{4c^2} (\sqrt{S_z(\Omega + \omega)} + \sqrt{S_z(\Omega - \omega)})^2 \quad (30)$$

We see from Eq. (30) that for $\Omega > \omega$ we have:

$$R(\Omega) = \frac{4c^2\omega^2}{E_0^2} \frac{S_x(\Omega)}{(\sqrt{S_z(\Omega + \omega)} + \sqrt{S_z(\Omega - \omega)})^2} \leq 1. \quad (31)$$

Introducing the magnitude $A_0 = E_0/\omega$ of the pulse vector potential, we can rewrite inequality (31) as:

$$\frac{S_x(\Omega)}{(\sqrt{S_z(\Omega + \omega)} + \sqrt{S_z(\Omega - \omega)})^2} \leq \frac{A_0^2}{4c^2} \quad (32)$$

The ratio $R(\Omega)$ defined in Eq. (31) is shown in Fig. 11(a) for the SR Yukawa potential and various pulse parameters. Of course, we cannot expect Eq. (31) to provide a rigorous upper bound since deriving it we neglected atomic potential in Eq. (27), which constitutes a rather drastic approximation. As one can see from Fig. 11(a) inequality (31) can indeed be violated. One can see, nevertheless, that Eq. (31), and consequently Eq. (32) provide reasonably accurate estimates of the relative magnitude of the intensities of the dipole and non-dipole harmonics.

While the non-zero expectation value v_x and appearance of the non-dipole harmonics is an entirely relativistic phenomena, the non-dipole effects also modify slightly the velocity component v_z . The magnitude of this effect is of the order of c^{-2} . This can be most easily seen from the Heisenberg equations of motion (26). The equation for $v_z(t)$ (the third of the equations (26)) contains the term $\hat{x}E(t)/c$ on the right-hand side. Since the expectation value of x is itself of the order of c^{-1} , the resulting effect on $v_z(t)$ is of the order of c^{-2} , which will produce a relativistic correction of the order of c^{-2} for the dipole harmonic intensity. We may expect, therefore, that the normalized difference:

$$\frac{\Delta S_z(\Omega)}{S_z(\Omega)} = \frac{S_z(\Omega) - S_z^{\text{nr}}(\Omega)}{S_z^{\text{nr}}(\Omega)}, \quad (33)$$

where $S_z(\Omega)$ is the dipole harmonics intensity obtained in the present TDDE calculation and $S_z^{\text{nr}}(\Omega)$ is the result of the non-relativistic TDSE calculation, should be of the order of c^{-2} . i.e., we may expect $\Delta S_z(\Omega)/S_z(\Omega) \sim 10^{-4}$. That this is indeed the case can be seen

from Fig. 11(b), where we show results of the TDDE and TDSE calculations performed for the same pulse parameters for the Yukawa atom.

The analysis based on the Heisenberg equations of motion (26) also allows to give a simple explanation for the behavior of $v_x(t)$ shown in Fig. 2, where the x - component of the electron velocity starts responding to the field only for the times approaching the midpoint of the pulse. Integrating Eq. (28) we obtain for the expectation value $v_x = \langle \phi_0 | \hat{v}_x | \phi_0 \rangle$ (assuming that it has zero value at $t = 0$):

$$v_x(t) = -\frac{1}{c} \int_0^t v_z(\tau) E(\tau) d\tau . \quad (34)$$

We could have obtained the same equation by integrating the first of the set of the classical equations (25), which is not surprising given the great formal similarity between the classical mechanics and the QM in the Heisenberg picture. We show in Fig. 12(a) the expectation value $v_z(t)$ obtained in the LOPT calculation for the cosine pulse with $E_0 = 0.0534$ a.u. and $\omega = 0.057$ a.u. We show only the LOPT result. Just as in the case of $v_x(t)$, shown in Fig. 2, the TDDE and LOPT results for $v_z(t)$ differ very slightly. In Fig. 12(b) we show the LOPT expectation value $v_x(t)$, as well as the estimate for $v_x(t)$ that we obtain if we substitute the LOPT value for $v_z(\tau)$ under the integral sign in Eq. (34). One can see that the estimate thus obtained reproduces fairly well the general behavior of $v_x(t)$. In particular, it reproduces the feature that we mentioned above: the x -component of the velocity begins deviating from zero appreciably only for the times approaching the midpoint of the pulse. We remind that effect of the atomic potential on the motion in the x -direction was neglected in the Heisenberg equation of motion (28) which we used to obtain the estimate (34). The fact that the estimate (34) reproduces qualitative behavior of the x -component of electron velocity shown in Fig. 2 tells us, therefore, that this behavior is a result of the interplay of the motion in x - and z - directions which are mutually interconnected due to presence of the Lorentz force.

IV. CONCLUSION

We have presented results of the relativistic calculations of even harmonic generation from various atomic targets. Our approach was based on the numerical solution of the TDDE. The

HHG spectra of the non-dipole even order harmonics were found to look qualitatively similar to the spectra of the dipole harmonics, obeying the same classical cutoff rules. The temporal formation of the non-dipole harmonics, however, was found to be quite different. The results of the Gabor transform analysis show that formation of the non-dipole harmonics is strongly suppressed at the beginning of the laser pulse, and bursts of the non-dipole radiation are shifted in time with respect to the bursts of the dipole emission. These features are partly explained by a simple generalization of the classical three-step model, which takes into account the selection rules governing emission of harmonic photons. We modeled the effect of these selection rules by using a filter parameter, which selects the trajectories with angular momentum exceeding a certain threshold value at the recollision time.

For the field parameters we considered the relativistic effects are still relatively weak and could be described perturbatively. LOPT provides, as we have seen, an adequate description of the non-dipole effects responsible for the even order harmonics emission. Use of the TDDE, however, is technically simpler than the calculations based on the LOPT, and opens the perspective of making an excursion into the truly relativistic domain in the future. We relied, therefore, on the TDDE-based approach in the present work. The present approach can also be generalized relatively easily to include some quantum electrodynamical (QED) effects, such as the vacuum polarization effects, or the QED strong Coulomb field radiative corrections, which can be taken into account by using effective potentials such as the Uehling potential [55, 56] or the radiative potential proposed in [57]. The procedure we apply to solve the Dirac equation can also be used to study the process of electron-positron pair production (PP) in strong electromagnetic fields, which occurs when field strength reaches the characteristic Schwinger field strength of 1.3×10^{16} V/cm. The process of PP in both homogeneous and inhomogeneous electric fields has received considerable interest in the literature [58]. Theoretical treatment of PP in the semiclassical approximation relies on a solution of the TDDE for a given field configuration [59]. Our procedure might prove useful for this purpose, especially in the case of the spatially inhomogeneous field, which has been found to play an important role in the PP [58, 60].

The numerical procedure we employ can be relatively easily generalized for the case of the many-electron relativistic Hamiltonians used in the quantum chemistry calculations [61, 62]. Use of the representation of the wave-function analogous to the expansion (6) would be, of course, impractical for systems with more than one electron if we want to use

such expansions to represent the wave-function in the whole space. One may use, however, the idea of the R -matrix approach, which separates the coordinate space in the inner region, where a suitable basis set representation can be used to represent many-electron wave-functions and the outer region, where one has to concentrate on the description of a single electron motion, for which the finite difference method might be better suited. Such a strategy has been implemented with success in the framework of the so-called R-Matrix incorporating Time method (RMT) [63] which allows to solve the non-relativistic TDSE for many-electron systems. One can use a similar approach in the relativistic case, relying on the results of the stationary quantum chemistry calculations [61, 62] for the description of the inner region, where many-electron effects are important, and using the present procedure to solve the TDDE describing electron propagation in the outer region.

Acknowledgments

This work was supported by the Institute for Basic Science grant (IBS-R012-D1) and the National Research Foundation of Korea (NRF), grant funded by the Korea government (MIST) (No. 2022R1A2C3006025). Computational works for this research were performed on the IBS Supercomputer Aleph in the IBS Research Solution Center.

-
- [1] H. R. Reiss, *Opt. Express* **2**, 261 (1998).
 - [2] H. R. Reiss, *J. Opt. Soc. Am. B* **7**, 574 (1990).
 - [3] A. Ludwig, J. Maurer, B. W. Mayer, C. R. Phillips, L. Gallmann, and U. Keller, *Phys. Rev. Lett.* **113**, 243001 (2014).
 - [4] S. Chelkowski, A. D. Bandrauk, and P. B. Corkum, *Phys. Rev. Lett.* **113**, 263005 (2014).
 - [5] S. Chelkowski, A. D. Bandrauk, and P. B. Corkum, *Phys. Rev. A* **92**, 051401(R) (2015).
 - [6] I.A.Ivanov, J. Dubau, and K. T. Kim, *Phys. Rev. A* **94**, 033405 (2016).
 - [7] V. S. Popov, B. M. Karnakov, V. D. Mur, and S. G. Pozdnyakov, *Sov. Phys. -JETP* **102**, 760 (2006).
 - [8] M. Klaiber and K. Z. Hatsagortsyan, *Phys. Rev. A* **90**, 063416 (2014).
 - [9] E. Yakaboylu, M. Klaiber, and K. Z. Hatsagortsyan, *Phys. Rev. A* **91**, 063407 (2015).

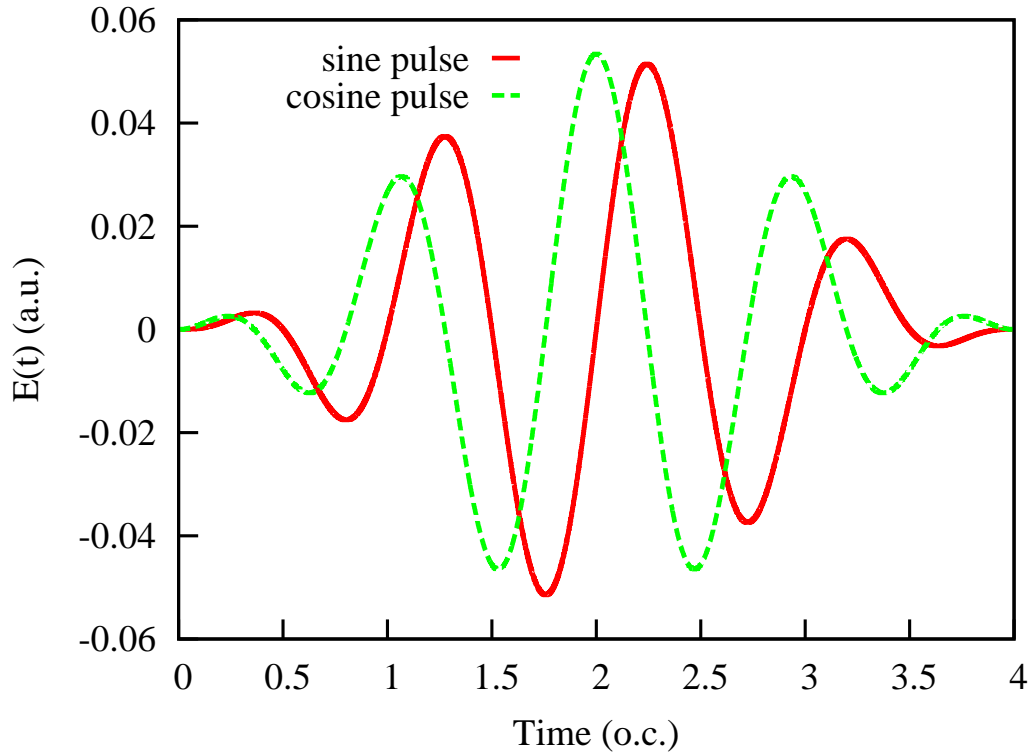


FIG. 1: (Color online) Pulse shapes $E(t)$ employed in the calculations.

- [10] L. V. Keldysh, Sov. Phys. -JETP **20**, 1307 (1965).
- [11] C. T. L. Smeenk, L. Arissian, B. Zhou, A. Mysyrowicz, D. M. Villeneuve, A. Staudte, and P. B. Corkum, Phys. Rev. Lett. **106**, 193002 (2011).
- [12] A. Ludwig, J. Maurer, B. W. Mayer, C. R. Phillips, L. Gallmann, and U. Keller, Phys. Rev. Lett. **113**, 243001 (2014).
- [13] F. Krausz and M. Ivanov, Rev. Mod. Phys. **81**, 163 (2009).
- [14] S. Chelkowski and A. D. Bandrauk, Phys. Rev. A **97**, 053401 (2018).
- [15] S. Chelkowski, A. D. Bandrauk, and P. B. Corkum, Phys. Rev. A **95**, 053402 (2017).
- [16] C. T. L. Smeenk, L. Arissian, B. Zhou, A. Mysyrowicz, D. M. Villeneuve, A. Staudte, and P. B. Corkum, Phys. Rev. Lett. **106**, 193002 (2011).
- [17] H. R. Reiss, Phys. Rev. A **87**, 033421 (2013).
- [18] E. Yakaboylu, M. Klaiber, H. Bauke, K. Z. Hatsagortsyan, and C. H. Keitel, Phys. Rev. A **88**, 063421 (2013).
- [19] S. Chelkowski and A. D. Bandrauk, Molecular Physics **115**, 1971 (2017).

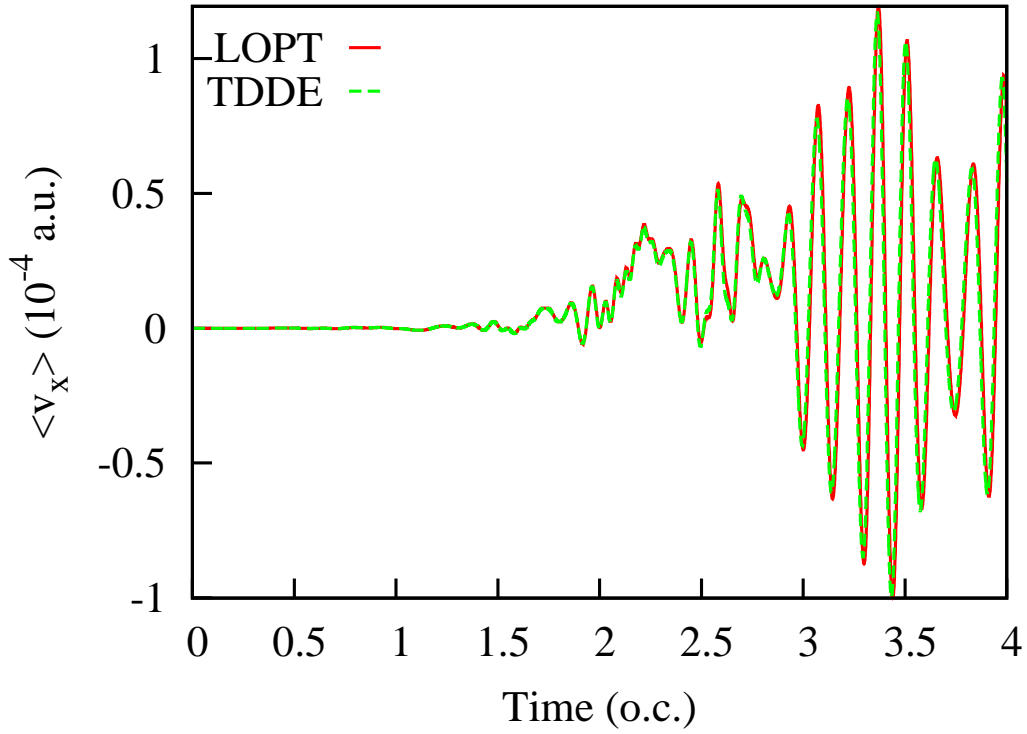


FIG. 2: (Color online) Expectation value of the x - component of the electron velocity as a function of time obtained in TDDE and LOPT calculations Cosine pulse with $E_0 = 0.0534$ a.u., $\omega = 0.057$ a.u. has been used in the calculation.

- [20] S. V. B. Jensen, M. M. Lund, and L. B. Madsen, Phys. Rev. A **101**, 043408 (2020).
- [21] D. A. Telnov and S.-I. Chu, Phys. Rev. A **102**, 063109 (2020).
- [22] S. Selstø, E. Lindroth, and J. Bengtsson, Phys. Rev. A **79**, 043418 (2009).
- [23] I.A.Ivanov, Phys. Rev. A **91**, 043410 (2015).
- [24] I. A. Ivanov, Phys. Rev. A **96**, 013419 (2017).
- [25] X. Zhu and Z. Wang, Optics Communications **365**, 125 (2016).
- [26] R. M. Potvliege, N. J. Kylstra, and C. J. Joachain, J. Phys. B **33**, L743 (2000).
- [27] N. J. Kylstra, R. M. Potvliege, and C. J. Joachain, J. Phys. B **34**, L55 (2001).
- [28] C. C. Chirilă, N. J. Kylstra, R. M. Potvliege, and C. J. Joachain, Phys. Rev. A **66**, 063411 (2002).
- [29] M. Lewenstein, P. Balcou, M. Y. Ivanov, A. L’Huillier, and P. B. Corkum, Phys. Rev. A **49**, 2117 (1994).
- [30] P. B. Corkum, Phys. Rev. Lett. **71**, 1994 (1993).

- [31] J. R. V. de Aldana and L. Roso, *J. Phys. B* **35**, 1633 (2002).
- [32] A. D. Bandrauk and H. Z. Lu, *Phys. Rev. A* **73**, 013412 (2006).
- [33] W. Mu-Xue, C. Si-Ge, L. Hao, and P. Liang-You, *Chinese Physics B* **29**, 013302 (2020).
- [34] A. Sarsa, F. J. Gálvez, and E. Buendia, *J. Phys. B* **36**, 4393 (2003).
- [35] A. Akhiezer and V. Berestetskii, *Quantum Electrodynamics* (John Wiley & Sons, 1965).
- [36] E. M. Lifshitz and V. B. Berestetskii, *Quantum Electrodynamics* (Pergamon Press, 1982).
- [37] M. Nurhuda and F. H. M. Faisal, *Phys. Rev. A* **60**, 3125 (1999).
- [38] R. N. Hill and C. Krauthauser, *Phys. Rev. Lett.* **72**, 2151 (1994).
- [39] P. A. M. Dirac, *The Principles of Quantum Mechanics* (McGraw-Hill, New York, 1964).
- [40] I. A. Ivanov and K. T. Kim, *Phys. Rev. A* **92**, 053418 (2015).
- [41] L. Shampine, *Numerical Solution of Ordinary Differential Equations* (Chapman & Hall, New York, NY, 1994).
- [42] A. Goldberg, H. M. Schey, and J. L. Schwartz, *Am. J. Phys.* **35**, 177 (1967).
- [43] P. Lambropoulos and D. Petrosyan, *Fundamentals of Quantum Optics and Quantum Information* (Springer-Verlag, Berlin, 2007).
- [44] I. I. Sobelman, *Introduction to the Theory of Atomic Spectra* (Pergamon Press, New York, 1972).
- [45] I. A. Ivanov, *Phys. Rev. A* **90**, 013418 (2014).
- [46] H. K. Avetissian, A. G. Markossian, and G. F. Mkrtchian, arXiv: Atomic Physics (2011).
- [47] J. C. Baggesen and L. B. Madsen, *J. Phys. B* **44**, 115601 (2011).
- [48] R. Reiff, T. Joyce, A. Jaroń-Becker, and A. Becker, *J. Phys. Commun* **4**, 065011 (2020).
- [49] R. Mishra, D. Kalita, and A. Gupta, *Eur. Phys. J. D* **66**, 169 (2012).
- [50] D. Gabor, *J. Inst. Electr. Eng.* **93**, 429 (1946).
- [51] P. Antoine, B. Piraux, and A. Maquet, *Phys. Rev. A* **51**, R1750 (1995).
- [52] Y. Y. Tang, L. H. Yang, J. Liu, and H. Ma, *Wavelet Theory and Its Application to Pattern Recognition* (World Scientific, 2000).
- [53] B. Wang, T. Cheng, X. Li, P. Fu, S. Chen, and J. Liu, *Phys. Rev. A* **72**, 063412 (2005).
- [54] L. D. Landau and E. M. Lifshitz, *Quantum Mechanics* (Pergamon Press, New York, 1977).
- [55] E. A. Uehling, *Phys. Rev.* **48**, 55 (1935).
- [56] E. A. Uehling, *Physical Review* **48**, 55 (1935).
- [57] V. V. Flambaum and J. S. M. Ginges, *Phys. Rev. A* **72**, 052115 (2005).

- [58] H. Gies and K. Klingmüller, *Phys. Rev. D* **72**, 065001 (2005).
- [59] G. R. Mocken, M. Ruf, C. Müller, and C. H. Keitel, *Phys. Rev. A* **81**, 022122 (2010).
- [60] C. Kohlfürst, *Phys. Rev. D* **101**, 096003 (2020).
- [61] H. Nakai, *Bull. Chem. Soc. Jpn.* **94**, 1664 (2021).
- [62] W. Liu, *J. Chem. Phys.* **152**, 180901 (2020).
- [63] M. A. Lysaght, L. R. Moore, L. A. A. Nikolopoulos, J. S. Parker, H. W. van der Hart, and K. T. Taylor, *Journal of Physics: Conference Series* **388**, 012027 (2012).

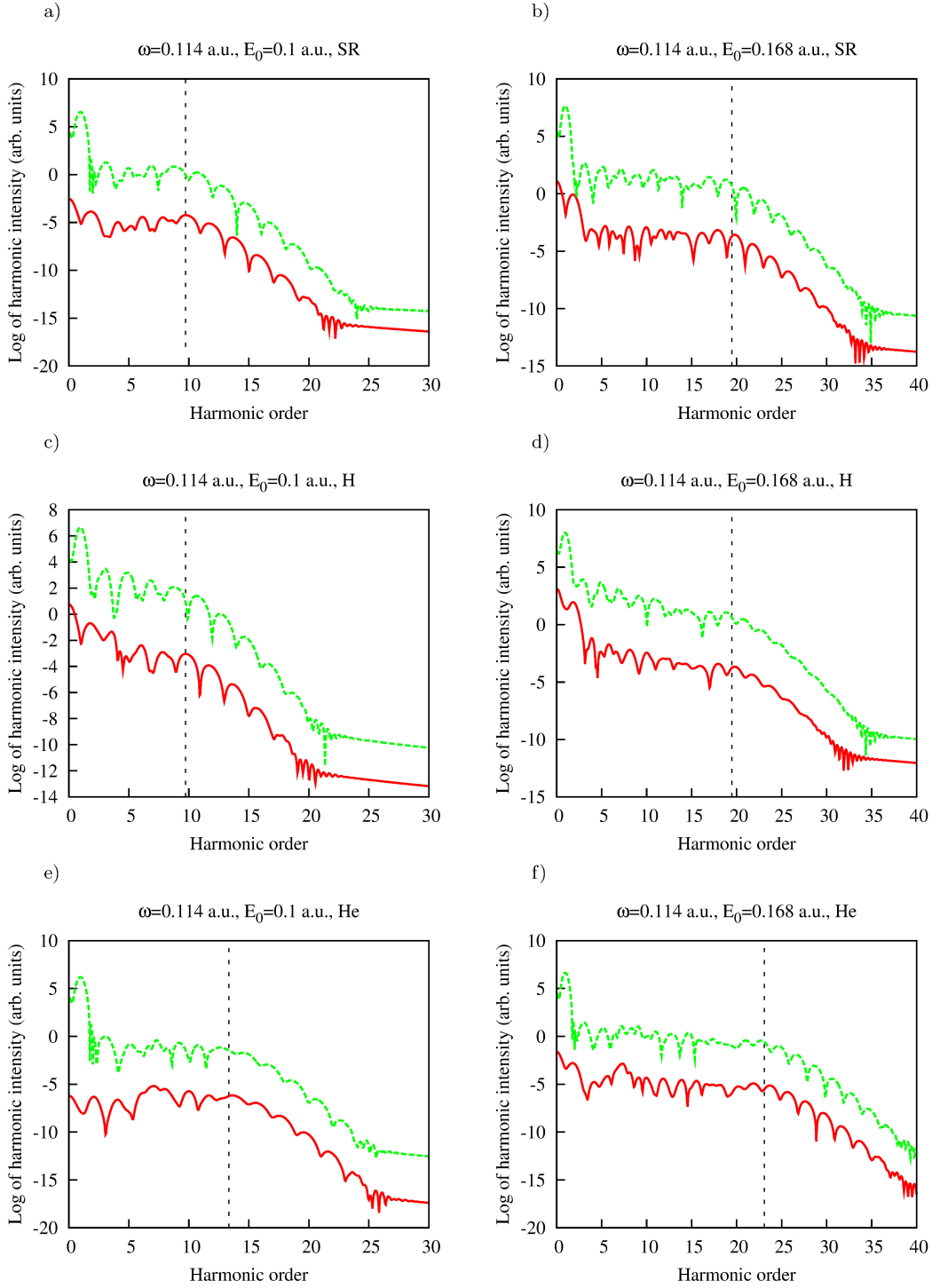


FIG. 3: (Color online) Dipole (dash green) and non-dipole (red solid) harmonic intensities for the pulse wavelength $\lambda = 400$ nm for the SR Yukawa, hydrogen and He atoms. Vertical dash lines show cutoff positions.

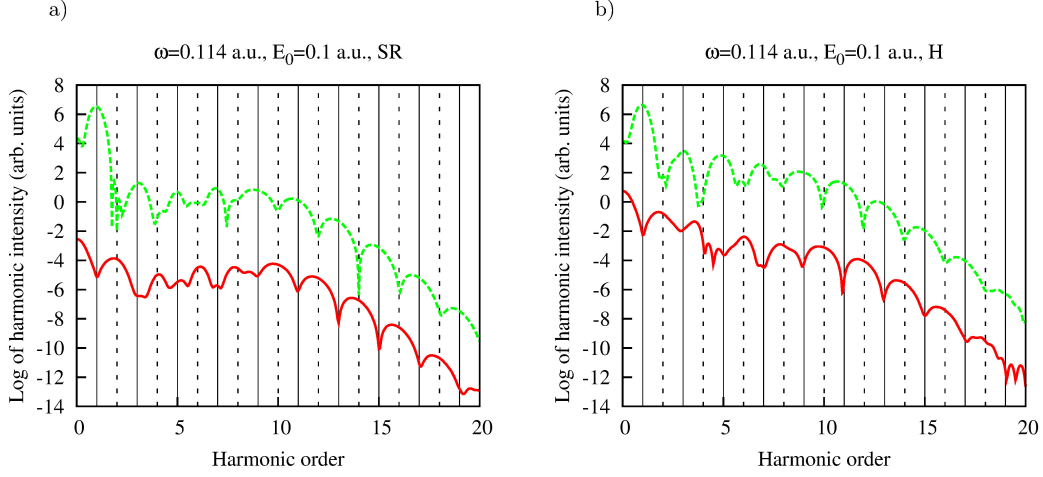


FIG. 4: (Color online) Dipole (dash green) and non-dipole (red solid) harmonic intensities for the pulse wavelength $\lambda = 400$ nm for harmonics with orders $n \leq 20$ for the SR Yukawa and hydrogen atoms. Vertical solid and dash lines show positions of odd and even harmonics, respectively.

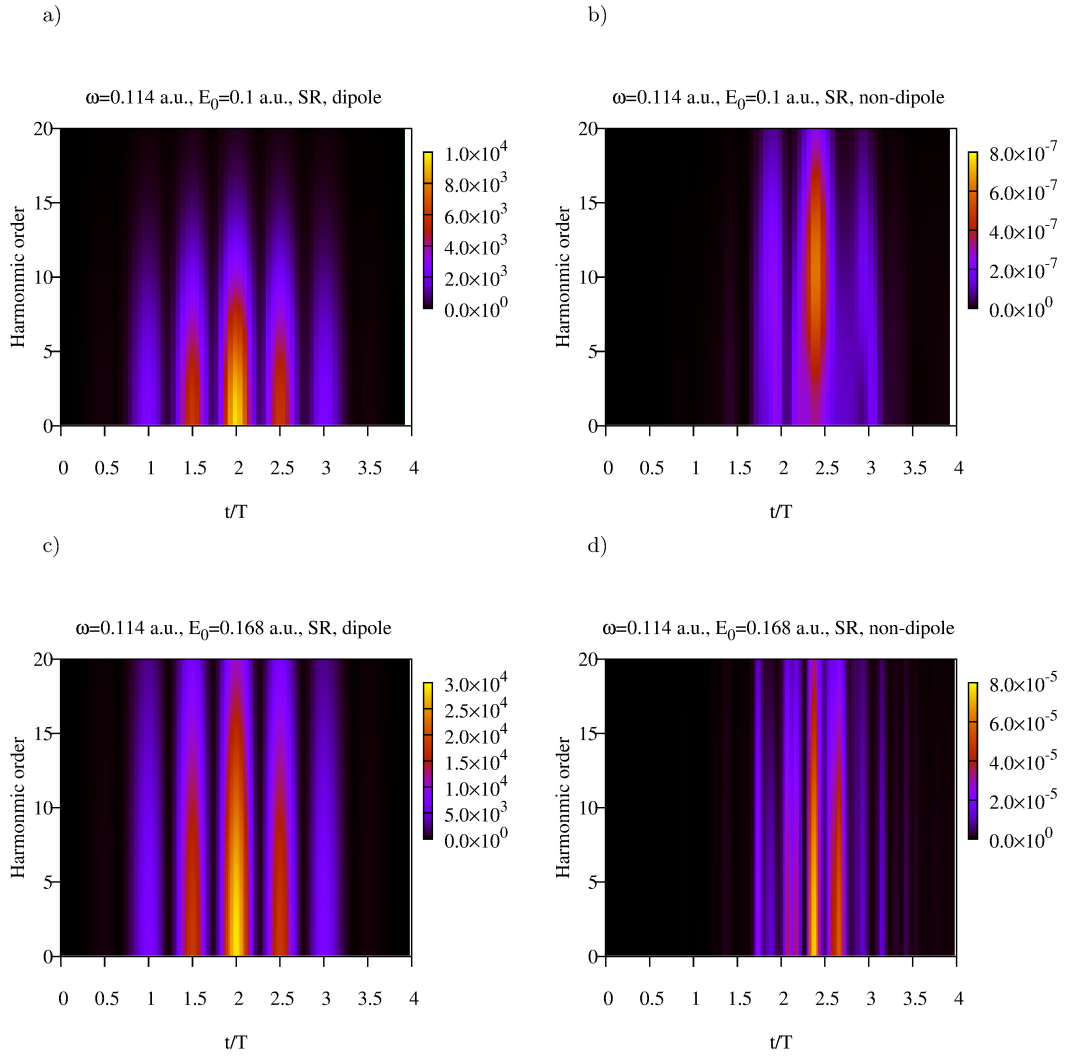


FIG. 5: (Color online) Gabor transform $|T(\Omega, t)|$ for the pulse wavelength $\lambda = 400$ nm and different field strengths for the SR Yukawa atom.

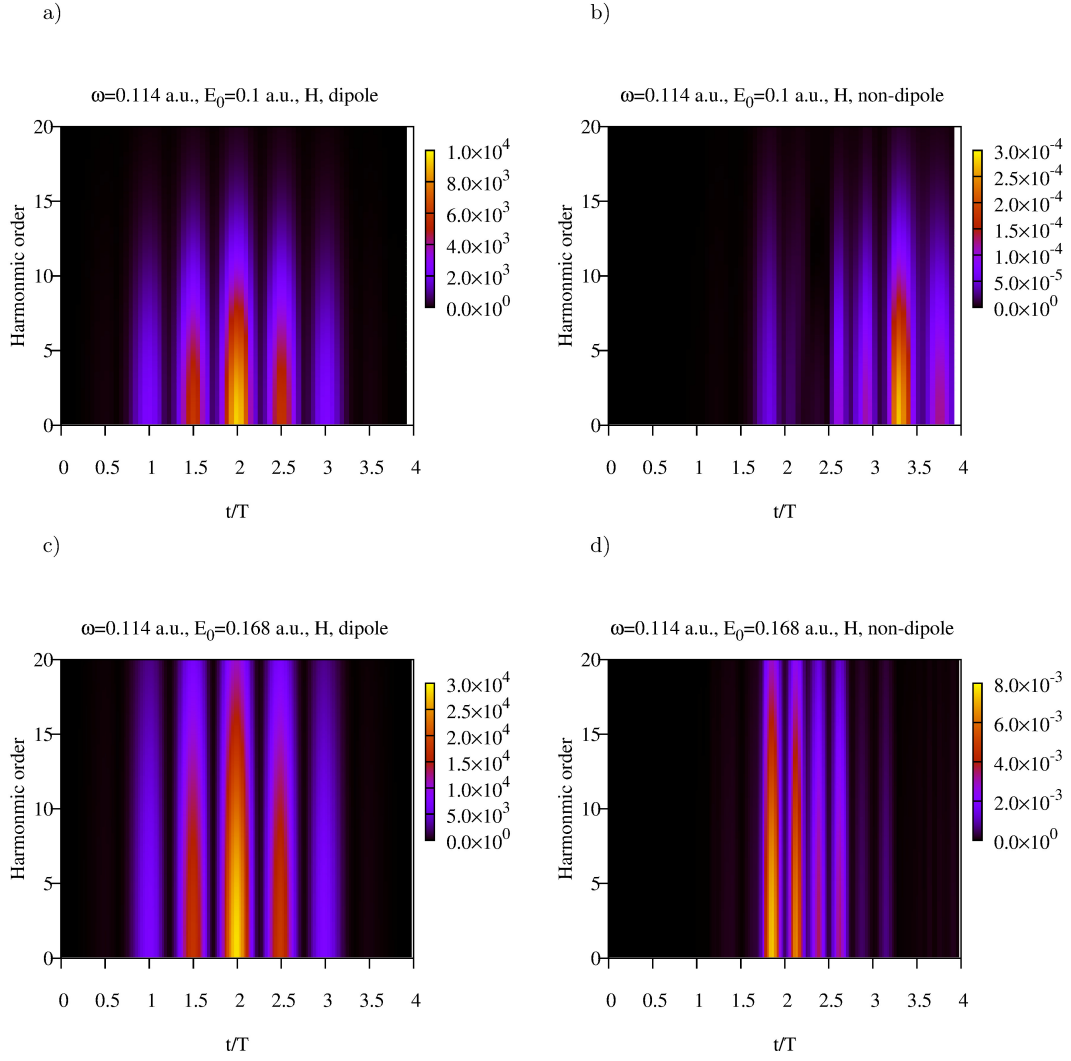


FIG. 6: (Color online) Gabor transform $|T(\Omega, t)|$ for the pulse wavelength $\lambda = 400$ nm and different field strengths for the hydrogen atom.

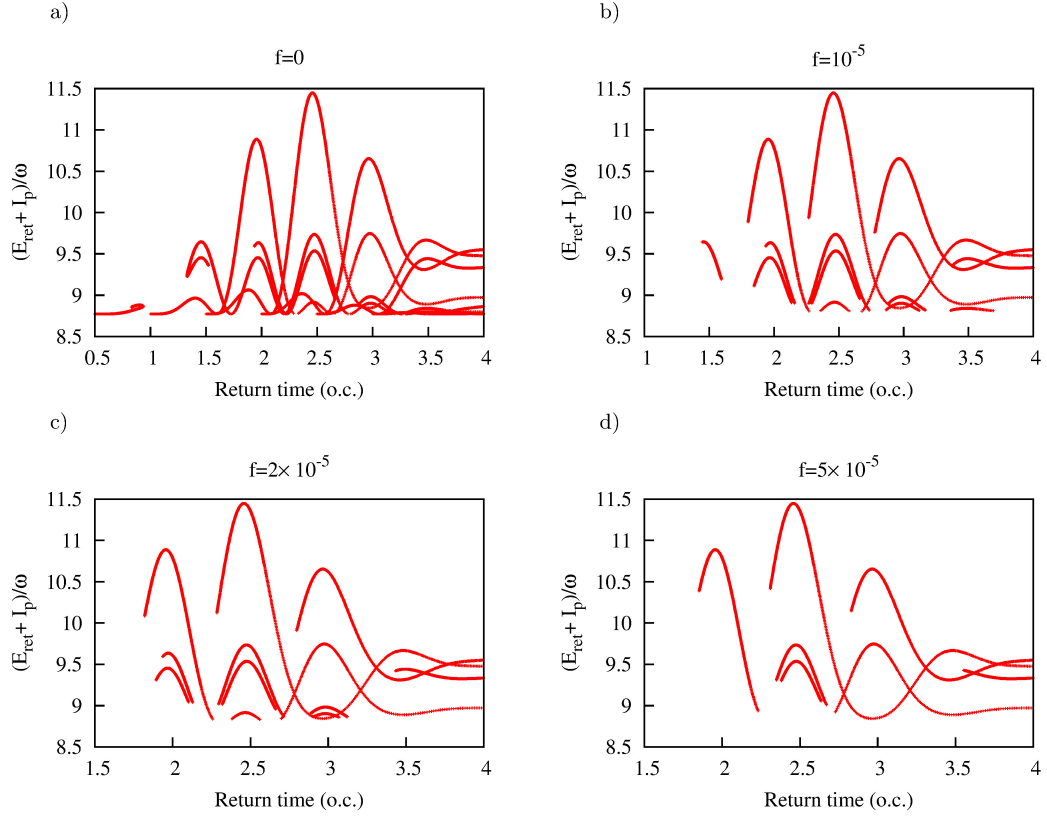


FIG. 7: (Color online) Classical calculations of emitted photon energy as function of return time for the dipole harmonic radiation (a) and non-dipole harmonic radiation (b-d) with different filter parameters.

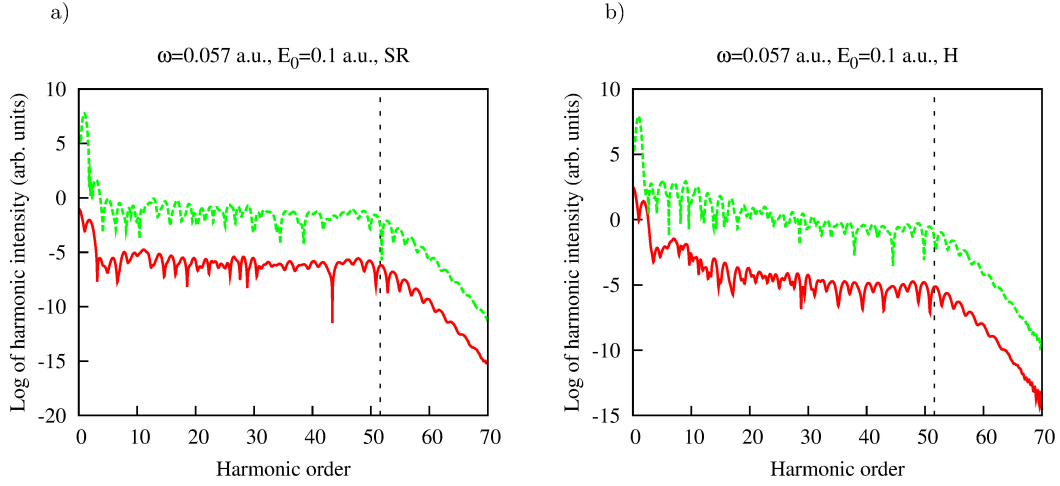


FIG. 8: (Color online) Dipole (dash green) and non-dipole (red solid) harmonic intensities for the pulse wavelength $\lambda = 800$ nm. for the SR Yukawa and hydrogen atoms. Vertical dash lines show cutoff positions.

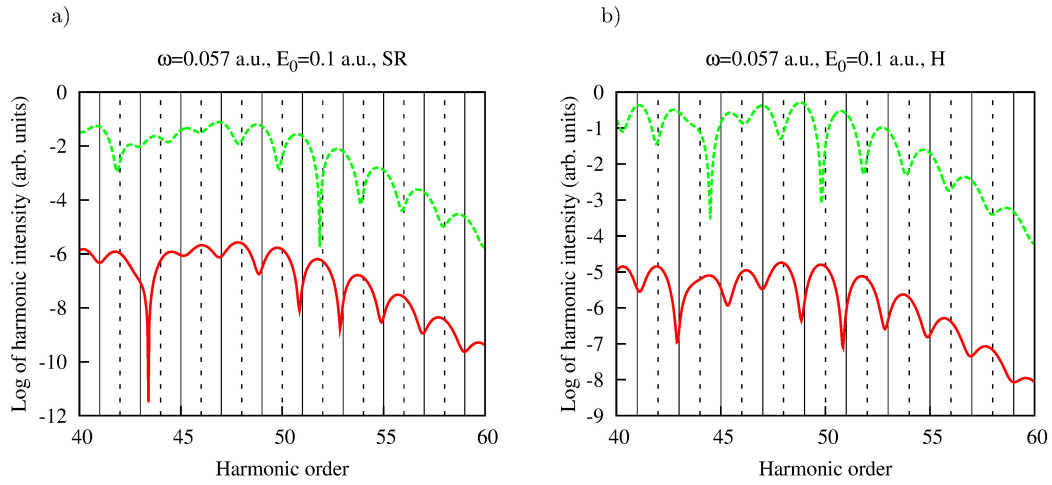


FIG. 9: (Color online) Dipole (dash green) and non-dipole (red solid) harmonic intensities for the pulse wavelength $\lambda = 800$ nm for harmonics with orders $40 \leq n \leq 60$ for the SR Yukawa and hydrogen atoms. Vertical solid and dash lines show positions of odd and even harmonics, respectively.

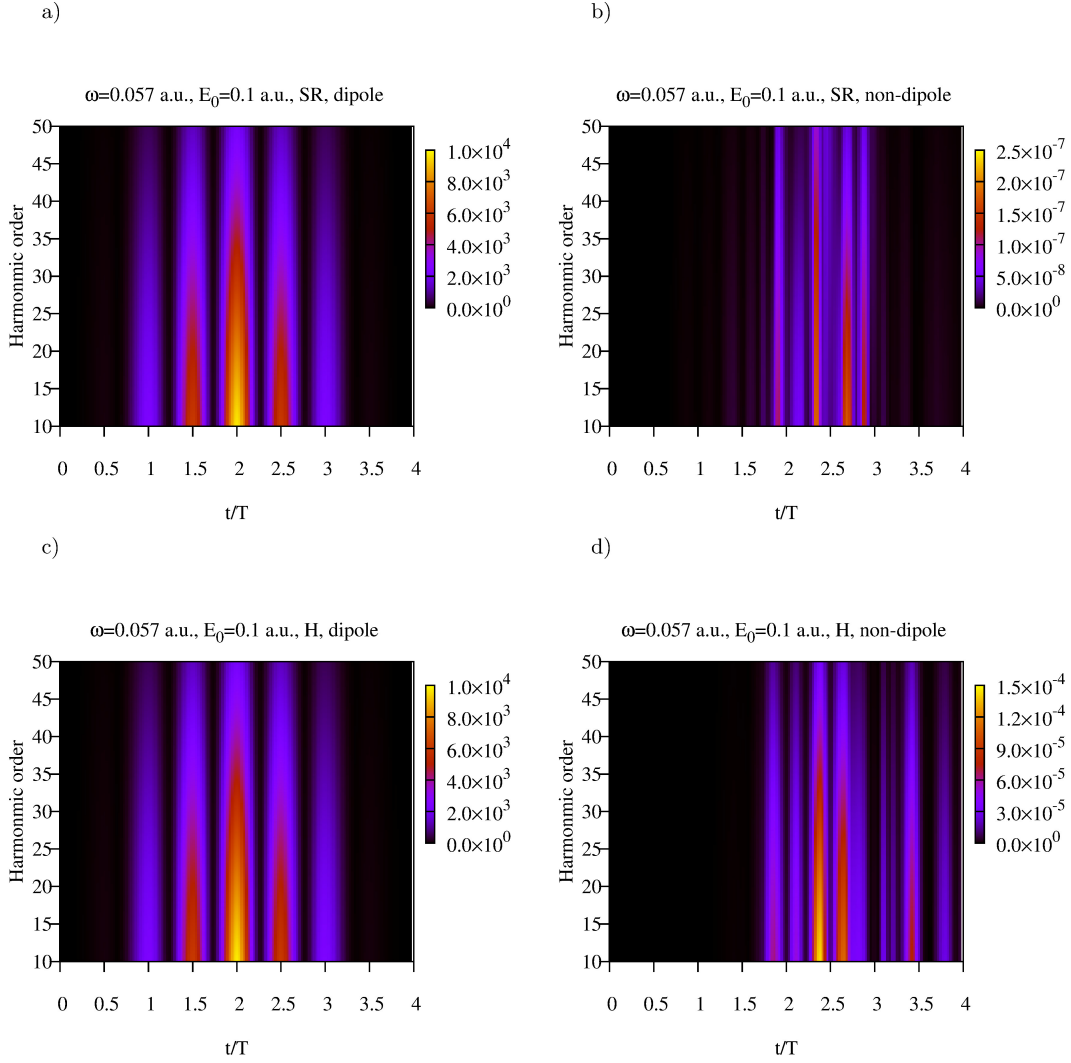


FIG. 10: (Color online) Gabor transform $|T(\Omega, t)|$ for the pulse wavelength $\lambda = 800$ nm for the SR Yukawa and hydrogen atoms.

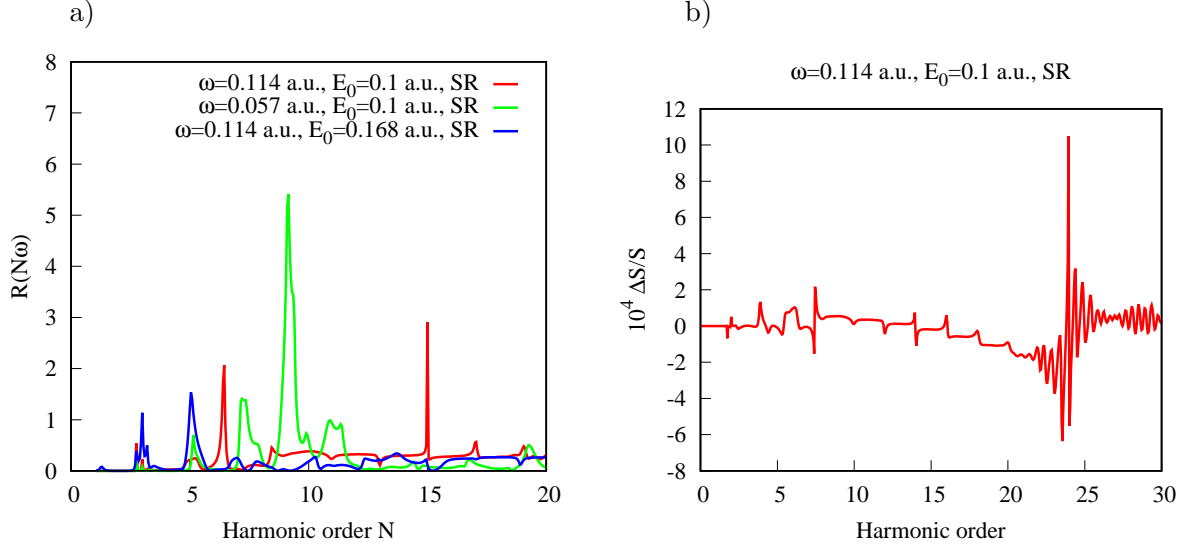


FIG. 11: (Color online) (a) Estimate (31) for the ratio $R(\Omega)$. (b) Normalized difference $(S_z(\Omega) - S_z^{\text{nr}}(\Omega))/S_z^{\text{nr}}(\Omega)$ of the TDDE and TDSE calculations for the dipole harmonic intensities.

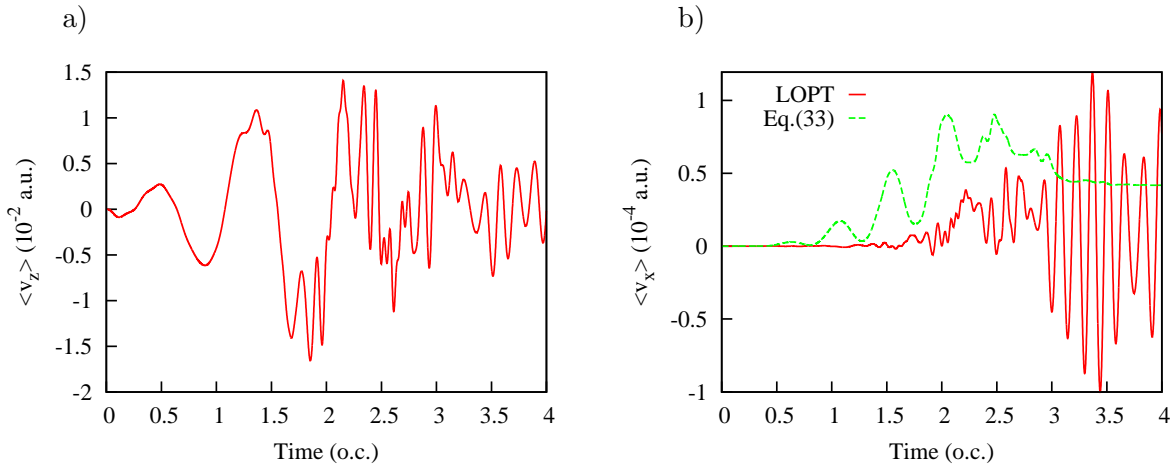


FIG. 12: (Color online) (a) LOPT expectation value $v_z(t)$. (b) $v_x(t)$ obtained in the LOPT calculation and using Eq. (34). Cosine pulse with $E_0 = 0.0534$ a.u., $\omega = 0.057$ a.u. has been used in the calculations.